Atmospheric correction on CCD data of HJ-1 satellite and analysis of its effect

ZHENG Sheng[1, 2], ZHAO Xiang[3], ZHANG Hao[1], HE Qisheng[1, 2], CAO Chunxiang[1], CHEN Liangfu[1]

1. *State Key Laboratory of Remote Sensing Science*, *Jointly Sponsored by the Institute of Remote Sensing Applications of Chinese Academy of Sciences and Beijing Normal University*, *Beijing* 100101, *China*;
2. *Graduate University of Chinese Academy of Sciences*, *Beijing* 100049, *China*;
3. *College of Resources Science & Technology*, *Beijing Normal University*, *Beijing* 100875, *China*

Abstract: The radioactive transfer process in the surface-atmosphere-remote sensor can be simulated by the atmospheric radioactive transfer model MODTRAN 4, thus the top of the atmosphere (TOA) radiance with the corresponding atmospheric parameters can be acquired. Based on the look-up table (LUT) which is generated by simulation, the surface reflectance from CCD data of HJ-1 satellite can be retrieved. Then, the effect of atmospheric correction on CCD data of HJ-1 satellite is analyzed in terms of the spectral curves, comparison with MODIS surface reflectance products, and the normalized difference vegetation index(NDVI). The results show: (1) Atmospheric correction on CCD data of HJ-1 satellite can eliminate the "increase" effect of the atmosphere. (2) The reflectance of vegetation and settlement place from atmospheric corrected CCD data of HJ-1 satellite is well consistent with those from MODIS surface reflectance data products, with less than 20% in error between these two surface features for the four bands of CCD data of HJ-1 satellite. (3) The difference of NDVI between vegetation and other objects after atmospheric correction has been increased, which indicates the atmospheric correction can highlight the vegetation information.

Key words: HJ-1 satellite, atmospheric correction, MODTRAN 4, MODIS

CLC number: P407.4/TP751.1 **Document code:** A

Citation format: Zheng S, Zhao X, Zhang H, He Q S, Cao C X and Chen L F. 2011. Atmospheric correction on CCD data of HJ-1 satellite and analysis of its effect. *Journal of Remote Sensing*, **15**(4): 709–721

1 INTRODUCTION

Due to the fact that China is one of the countries with the most serious natural disasters, the satellite remote sensing monitoring system is demanded to strengthen the disaster monitoring, disaster warning, and disaster forecasting. Fortunately, HJ-1 satellite can play an important role in this area. The main missions of HJ-1 satellite are to monitor pollution, ecosystem destruction and natural disaster on large-scale dynamics and around the clock. In the meantime, it also forecasts development and changes of eco-environment and natural disaster and evaluates environmental quality and disaster damage immediately and scientifically (Wang & Wang, 2006; Wang, *et al.*, 2008). These missions of HJ-1 satellite are inseparable from the quantitative analysis of remote sensing. For example, in the eco-environment, we have vegetation index, leaf area index, soil water content and other geophysical variables through quantitative remote sensing. Atmospheric correction for remote sensing data is one of the basic processes in quantitative remote sensing. The extinction caused by the scattering of atmospheric molecules and aerosols, and the absorption of ozone and gases such as water vapor can greatly influence the signals received by sensors, the spaceborne and airborne remote sensing information therefore can not directly characterize the surface objects. Moreover, a large number of inversion algorithms are based on surface reflectance which is actually obtained after atmospheric correction. Therefore, atmospheric correction is an essential part in quantitative inversion of land surface parameters.

Current atmospheric correction models can generally be summarized as follows: image feature-based model, the linear regression model based on the prior knowledge of the ground, and theoretical models of atmospheric radiative transfer (Zhao, 2004). The image feature-based model just utilizes the information of the remote

Received: 2010-04-29; **Accepted**: 2010-08-02

Foundation: The National Research program (973 program) (No.2007CB714402); The National High Technology Research and Development Program of China(No.2008AA12Z107); Special Grant for Prevention and Treatment of Infectious Diseases (No.2008ZX10004-012)

First author biography: ZHENG Sheng (1988—), male, graduated from China University of Geosciences (Wuhan), majoring in geography information system in 2009, is a graduate student from Institute of Remote Sensing Applications of Chinese Academy of Sciences now. Currently, he is engaged in the applications of spatial information technologies in public health and remote sensing inversion of forest parameters. E-mail: zhengsheng1213@163.com

Corresponding author: ZHANG Hao(1974—), male, received the Ph.D. degree from Beijing Normal University, is an associate professor from Institute of Remote Sensing Applications of Chinese Academy of Sciences. Currently, he is engaged in remote sensing inversion of forest parameters. E-mail: zhangh@irsa.ac.cn

CAO Chunxiang(1964—), female, professor of Institute of Remote Sensing Applications of Chinese Academy of Sciences. She received the Ph.D. degree from Hiroshima University. Her interests are the applications of spatial information technologies in public health and remote sensing inversion of forest parameters. E-mail: cao413@irsa.ac.cn

sensing images, so there are large noises in the corrected images by means of this model at different levels. The linear regression model based on the prior knowledge of the ground requires the ground spectral measurements synchronously at the calibration point, on top of which the calibration point should both be uniform and small. The theoretical models of atmospheric radiative transfer can describe the scattering, absorption process of the atmosphere reasonably, and it is based on the accurate radiative transfer models and available methods of obtaining atmospheric parameters. The current radiative transfer models include MODTRAN, ACORN, HATCH, *etc* (Matthew, *et al.*, 2002).

MODTRAN model is an improved version of LOWTRAN model by increasing the spectral resolution of LOWTRAN model from 20 cm^{-1} to 2 cm^{-1}, which includes a molecular absorption algorithm with the 2 cm^{-1} spectral resolution and the improved treatment of the relationship between the atmospheric pressure and the temperature of the molecular absorption. Also, it maintains basic procedures and structures of LOWTRAN 7 model. In the program processing, MODTRAN model basically follows the structure of LOWTRAN model, and can be used as the choice of the computing power in the middle spectral resolution without interfering the original implementation. MODTRAN model is better than LOWTRAN when the atmosphere height is higher than 30 km. The input parameters of the MODTRAN model can be divided into five categories: satellite operation parameters, sensor parameters, atmospheric parameters, observation geometry and surface parameters (Berk, *et al.*, 1999; Wu, *et al.*, 1998).

In this paper, we apply the atmospheric radiative transfer model MODTRAN 4 to conduct atmospheric correction on CCD data of HJ-1 satellite. The apparent radiance under the corresponding atmospheric parameters can be simulated by MODTRAN 4, which are further used to built the look-up table. Thereafter, atmospheric correction on CCD data of HJ-1 satellite is achieved pixel by pixel. After that, the effect of atmospheric correction on CCD data of HJ-1 satellite is discussed in terms of the spectral curves, comparison with MODIS surface reflectance products, and the NDVI.

2 THEORY OF ATMOSPHERIC CORRECTION

The airborne imaging process more or less follows the path like this: the signals reflected by the land surface penetrate the atmosphere before returning to satellite sensor; during the process they will suffer atmospheric extinction due to the scattering and absorption. Therefore, the signals received by the sensor are mixed. Applying the radiative transfer model MODTRAN 4 to simulate this process, we can retrieve the surface reflectance from CCD data onboard HJ-1 satellite. During the inversion process, there are three main variables involved: apparent radiance, apparent reflectance, surface reflectance.

2.1 Apparent radiance computation

Computing the apparent radiance is meant to utilize the calibration coefficients to convert the DN values of the original images to apparent radiance, which is the basis of quantitative inversion. Application of remote sensing data depends largely on the accuracy of the calibration coefficients. DN values can be converted to apparent radiance through Eq. (1).

$$L_\lambda = (DN / gain) + bias \tag{1}$$

where L_λ denotes the measured apparent radiance; *DN* refers to pixel value in the original image; *gain* is sensor's corresponding gain; *bias* is sensor's corresponding bias. For the CCD data of HJ-1 satellite, the calibration coefficients can be acquired from the metadata file, which are included in the downloaded data. The CCD1 data of HJ-1A satellite are used in this paper when applying the effect analysis of atmospheric correction, and the corresponding calibration coefficients are showed in Table 1.

Table 1 Correction coefficients of HJ-1A CCD1

	Band1 (0.41—0.52 μm)	Band2 (0.52—0.60 μm)	Band3 (0.63—0.69 μm)	Band4 (0.76—0.90 μm)
Gain($DN/W \cdot m^{-2} \cdot sr^{-1} \cdot \mu m^{-1}$)	0.5763	0.5410	0.6824	0.7209
Bias($W \cdot m^{-2} \cdot sr^{-1} \cdot \mu m^{-1}$)	9.3183	9.1758	7.5072	4.1484

2.2 Algorithm of Apparent reflectance

Upon implementing the radiometric calibration of the remote sensed images, we can convert apparent radiance to apparent reflectance through Eq. (2). The apparent radiance L_λ in the Eq. (2) denotes the spectral radiance from the top of the atmosphere into the satellite sensor, and it includes both the surface radiance and the atmospheric radiance. Therefore, the apparent reflectance on top of the atmosphere is also the sum of the surface reflectance and the atmospheric reflectance (Chi, *et al.*, 2005). Therefore, the effect of atmospheric correction can be analyzed through comparing the apparent reflectance and surface reflectance.

$$\rho_\lambda = \frac{\pi L_\lambda d^2}{ESUN_\lambda \cos\theta_s} \tag{2}$$

In the Eq. (2), ρ_λ represents the apparent reflectance of λ-band. L_λ refers to the apparent radiance of λ-band. *d* is the Earth-Sun distance in astronomical unit, and the value can be obtained through interpolating values in Table 2 (Landsat Project Science Office, 2009). $ESUN_\lambda$ is the solar spectral irradiance of λ-band in the upper atmosphere, and the value can be calculated from the CCD data's spectral response functions and the sun illumination data. $ESUN_\lambda$ used in this paper is showed in table 3. θ_s denotes the sun zenith angle (Zhao, *et al.*, 2007).

Table 2 Earth-Sun Distance in Astronomical Unit

Day of year	Distance	Day of year	Distance	Day of year	Distance	Day of year	Distance	Day of year	Distance
1	0.98331	74	0.99446	152	1.01403	227	1.01281	305	0.99253
15	0.98365	91	0.99926	166	1.01577	242	1.00969	319	0.98916
32	0.98536	106	1.00353	182	1.01667	258	1.00566	335	0.98608
46	0.98774	121	1.00756	196	1.01646	274	1.00119	349	0.98426
60	0.99084	135	1.01087	213	1.01497	288	0.99718	365	0.98333

Table 3 Solar spectral irradiance(w/(m^2.μm)) in the upper atmosphere for CCD data of HJ-1 satellite

	Band1 (0.41—0.52 μm)	Band2 (0.52—0.60 μm)	Band3 (0.63—0.69 μm)	Band4 (0.76—0.90 μm)
HJ-1A CCD1	1914.324	1825.419	1542.664	1073.826
HJ-1A CCD2	1929.810	1831.144	1549.824	1078.317
HJ-1B CCD1	1902.188	1833.626	1566.714	1077.085
HJ-1B CCD2	1922.897	1823.985	1553.201	1074.544

2.3 Algorithm of surface reflectance

Based on the theory of radiative transfer, assuming that underlying surface is homogeneous Lambert, the radiance received by the sensor on top of the atmosphere can be expressed as Eq. (3) (Liang, *et al.*, 1997).

$$L_m = L_0 + \frac{\rho}{1-s\cdot\rho}\cdot\frac{TF_d}{\pi} \tag{3}$$

where L_0 denotes atmospheric radiance of zero land surface reflectance; T refers to transmittance from land surface to sensor; s is spherical albedo in the underlying atmosphere; ρ is pixel reflectance; F_d is downward radiation flux density which reaches land surface (Zhao, *et al.*, 2007).

For atmospheric correction on CCD data of HJ-1 satellite, two steps are involved in converting the apparent radiance L_m to surface reflectance ρ through Eq. (3). The first step is to obtain the corresponding atmospheric parameters. Solar zenith angle can be obtained indirectly from the header file. Satellite zenith angle can be obtained from the downloaded satellite zenith file. Horizontal meteorological range can be converted from the aerosol optical depth (He, *et al.*, 2003). There are many methods to get the aerosol optical depth. We can either refer to the dark target algorithm developed by Kaufman, *et al.* (1997) to retrieve the aerosol or directly download daily MODIS aerosol products to roughly estimate the aerosol optical depth in the study area. The second step is to retrieve the surface reflectance through Eq. (3). Firstly, MODTRAN 4 will be run for three times with some atmospheric parameters, and three different values of surface reflectance (namely, 0, 0.5, 0.8) are assumed. We can obtain three simulated apparent radiances L_m from the simulations. Then we substitute the three groups of surface ρ and apparent radiance L_m into Eq. (3), and we can establish a ternary linear equation set involving the variables L_0, s and TF_d/π. After solving the equation set, we can get L_0, s and TF_d/π which are all a function of the atmospheric parameters. Thus, for the three variables: atmospheric parameters, surface reflectance and the apparent radiance, we can obtain the third variable as long as two of them are known (Liang, *et al.*, 2001).

In this paper, we establish the look-up table through MODTRAN 4 by assuming that underlying surface is a homogeneous Lambert. Due to the differences in the spectral response functions for the four bands' of CCD data, we need to establish the look-up table for each band. The changes of horizontal meteorological range, water vapor content, solar zenith angle, satellite zenith angle and other parameters are usually taken into account during atmospheric correction. Because no water vapor absorption bands for CCD data, the impact of water vapor is little and is not considered. When establishing the look-up table, we refer to the look-up table of MODIS aerosol inversion established by Remer1 (2006), and we also interpolate some values to improve the accuracy of atmospheric correction. The independent variables of the four look-up tables include the atmospheric model, satellite zenith angle, solar zenith angle and horizontal meteorological range, and the dependent variables are L_0, s and TF_d/π in the Eq.(3). The atmospheric model can be 2 or 3, representing mid-latitude summer or mid-latitude winter, respectively. The satellite zenith angles are set to 0°, 8°, 16°, 24°, 32°; solar zenith angles are assigned to 0.0°, 6.0°, 12.0°, 24.0°, 35.2°, 48.0°, 54.0°, 60.0°, 66.0°; horizontal meteorological range is 0.4 km, 0.7 km, 0.9 km, 1.2 km, 1.4 km, 1.7 km, 2 km, 2.3 km, 2.6 km, 3.1 km, 3.5 km, 4.0 km, 4.4 km, 5.2 km, 6.1 km, 7.0 km, 7.9 km, 9.6 km, 11.4 km, 13.1 km, 16.6 km, 20.2 km, 23.7 km, 27.2 km, 33.8 km, 40.4 km, 53.6 km, 66.8 km, 80.0 km.

2.4 Conversion between aerosol optical depth and horizontal meteorological range

Aerosol optical depth is widely used in atmospheric correction. For example, the MODIS aerosol optical depth product has been used as one of the input parameters of atmospheric correction (King, *et al.*, 1992). However, the required input parameter is horizontal meteorological range in MODTRAN 4, which is one of the independent variables in the look-up table. Therefore, we need to convert the aerosol optical depth to horizontal meteorological range during atmospheric correction. According to Lambert-Beer law, we use the following Eq. (He, *et al.*, 2003).

$$\tau_a = \int_{z_1}^{z_2} N(z,VIS)\cdot EXT(\lambda)m_a(z)\mathrm{d}z = -\ln T_a \tag{4}$$

where τ_a denotes aerosol optical depth; $N(z, VIS)$ is aerosol particle density coefficient related to height (z) and horizontal meteorological range; $EXT(\lambda)$ is extinction coefficient; λ is wavelength; $m_a(z)$ is atmospheric quality; τ_a is transmittance caused by aerosol (Zhao, *et al.*, 2007). We can calculate the aerosol's transmittance under different horizontal meteorological ranges, seasons, water vapor contents and aerosol modes with MODTRAN 4 to acquire the aerosol optical depth. Thus the relation between horizontal meteorological range and aerosol optical depth is established. As the water vapor effect on the relationship between the two is little (He, *et al.*, 2003), it is not considered. Selecting rural aerosol, and dividing seasons into spring with summer and autumn with winter, we obtain the relationship between aerosol optical depth and horizontal meteorological range in rural aerosol properties and two different seasons. Fig. 1 shows the curve fitting between aerosol optical depth and horizontal meteorological range in summer and in rural aerosol, and Fig. 2 shows the curve fitting between inverse aerosol optical depth and horizontal meteorological range in summer and in rural aerosol. By means of linear regression analysis of software SPSS (Mi & Zhang, 2000), the coefficients of curve fitting between inverse aerosol optical depth and horizontal meteorological range in summer and in rural aerosol can be obtained.

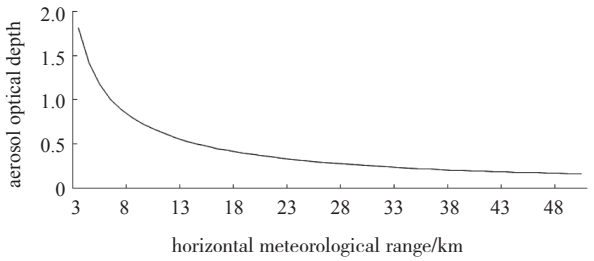

Fig. 1 The curve fitting between aerosol optical depth and horizontal meteorological range in summer and in rural aerosol

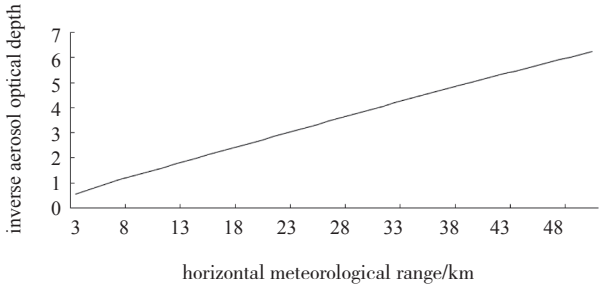

Fig. 2 The curve fitting between inverse aerosol optical depth and horizontal meteorological range in summer and in rural aerosol

The fitting result shows are shown as follows:

spring to summer

$$\frac{1}{t(550)} = 0.1202V + 0.29735 \tag{5}$$

and autumn to winter

$$\frac{1}{t(550)} = 0.1419V + 0.1377 \tag{6}$$

where $t(550)$ denotes the aerosol optical depth at 550 nm, and V refers to the horizontal meteorological range (km).

3 RESULTS AND ANALYSIS

In this paper, we estimate the surface reflectance of CCD1 data of HJ-1A satellite in Huzhou, Zhejiang Province on May 9, 2009. The study area is located around 30°48′ N, 120°6′ E. The solar zenith angle is 18°36′ and the atmospheric model used is mid-latitude summer with rural aerosol mode. According to the row-column numbers where the study area is located in the CCD1 data of HJ-1A satellite, we can get the satellite zenith angle of the study area which is 9° from the downloaded satellite zenith angle file. According to MODIS aerosol optical depth products, we find that the aerosol optical depth above the study area is 0.325, and horizontal meteorological range is 23.12 km. With these atmospheric parameters and MODTRAN 4, the look-up table is built and then atmospheric correction on CCD data of HJ-1 satellite can be achieved by means of VC^{++} programming.

3.1 Effect of atmospheric correction on the spectral characteristics of surface features

There are two ways that the atmosphere can influence ground targets' "brightness" or "radiance" recorded by remote sensors. One way is that atmospheric absorption and scattering will weaken the solar radiation energy which reaches the ground and the energy reflected from the target. The other way is that atmosphere is a reflector (scattering), which indicates that it will increase the atmospheric radiance of zero land surface reflectance which in fact contains no information of ground (Zhao, 2004). For visible bands, they are mainly influenced by the second way. In this paper, we analyze the apparent reflectance and surface reflectance on three typical surface features: water, vegetation, and settlement place.

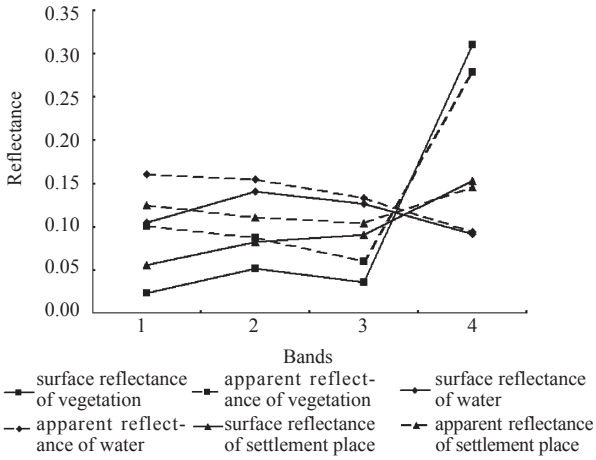

Fig. 3 The object spectrum from the surface reflectance and the apparent reflectance

As shown in Fig. 3, three surface features' spectral responses of apparent reflectance are higher than those of surface reflectance in blue band (band1), green band (band2), red band (band3). Taking vegetation for instance, comparing the date before and after correction, we find the largest change rate is 76.6% for blue band, followed by 41.1% for the green band, then 40.0% for red band through Eq. (7). This is because of the different selectivity of atmospheric scattering; it has larger impact on shortwave, but lower impact on long wavelength. Atmospheric correction eliminates the "increase" effect of atmospheric scattering in the visible bands.

$$k = \frac{|\rho_s - \rho_{toa}|}{\rho_{toa}} \cdot 100\% \tag{7}$$

In the Eq. (7), k denotes the rate of change; ρ_s is the surface reflectance after atmospheric correction; ρ_{toa} refers to the apparent reflectance before atmospheric correction; symbol "||" is to calculate the absolute value.

3.2 Compared with MODIS surface reflectance data products

To further verify the effect of atmospheric correction, we compare atmospheric corrected CCD data of HJ-1 satellite with MODIS surface reflectance products. Although the spatial resolution of the MODIS surface reflectance product is larger than that of CCD data, we can find pixels combined by one of these two surface features from the two kinds of data due to the wide range of vegetation and settlement place in the study area. Accordingly, no effect is observed owning to the spatial resolution differences when comparing the surface reflectance of the two kinds of data for study area. There are five kinds of MODIS surface reflectance products, and we use MOD09GA and MOD09GQ products (Vermote, *et al.*, 2008). MOD09GA provides MODIS band1-7 surface reflectance at 500-meter resolution. To improve the verification accuracy, we just use blue and green bands; red and near infrared bands are replaced

by MOD09GQ product which provides surface reflectance at 250-meter resolution. MOD09GA and MOD09GQ products are both acquired on May 9, 2009, and it is at the same time when HJ-1A CCD1 data is acquired.

It is necessary for us to preprocess the MODIS surface reflectance products before the comparison. Firstly, the projection of MODIS surface reflectance products is converted to WGS84 ellipsoid, UTM projection. Then, we clip the study area, and resample the 500-meter resolution of blue, green bands to the resolution of MOD09GQ. Lastly, we merge the four bands into one image file. The processing flow is showed as Fig. 4.

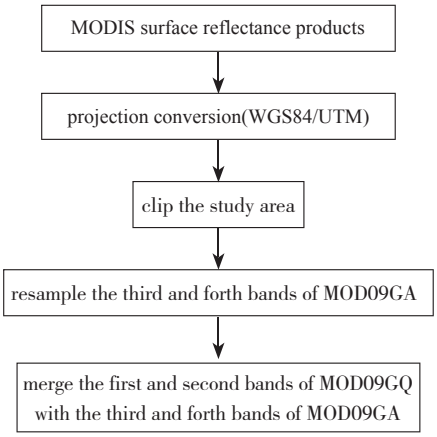

Fig. 4 The preprocessing flow of MODIS surface reflectance products

After resampling the resolution, we begin to compare CCD data of HJ-1 satellite with MODIS products. We select one pixel from the two surface features (vegetation and settlement place) randomly in the study area, and the reflectance values of the two pixels from two kinds of data are obtained that are showed in Fig. 5. We find that the surface reflectance of the two surface features from the two kinds of data is well consistent. According to the Eq. (8), we calculate the errors in Table 4, and we find vegetation's and settlement place's errors from the four bands of CCD data of HJ-1 satellite are within 20%.

$$e = \frac{|\rho_{\mathrm{HJCCD}} - \rho_{\mathrm{MODIS}}|}{\rho_{\mathrm{MODIS}}} \times 100\% \tag{8}$$

where e denotes the error; ρ_{HJCCD} refers to the surface reflectance from CCD data of HJ-1 satellite; ρ_{MODIS} refers to the surface reflectance from MODIS; symbol "||" is to calculate the absolute value.

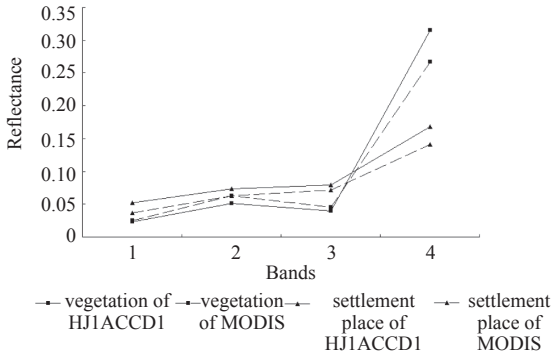

Fig. 5 The surface reflectance of the vegetation from HJ-1A CCD1 and MODIS on may 9, 2009

Table 4 Errors of surface reflectance between HJ-1A CCD1 and MODIS

/%

	Band1	Band2	Band3	Band4
Vegetation	7.4	18.6	12.1	18.0
settlement place	42.1	17.4	11.4	18.8

3.3 Effect of atmospheric correction on NDVI

Because vegetation index is a widely used variable in quantitative remote sensing, and remote sensing and ecological models which take remote sensing inputs as driving variables need the participation of vegetation index (Peng, *et al.*, 2007). In order to verify the effect atmospheric correction on CCD data of HJ-1 satellite, we compare the normalized difference vegetation index (NDVI) of before atmospheric correction with that of after atmospheric correction. Some studies (Abduwasit, *et al.*, 2004; Xu & Feng, 2007; Li, *et al.*, 2008) show that NDVI can verify the effect of atmospheric correction. The computational formulas of NDVI of before atmospheric correction and after atmospheric correction are showed as follows:

$$\mathrm{NDVI}_{\mathrm{TOA}} = \frac{TOA_{\mathrm{NIR}} - TOA_{\mathrm{RED}}}{TOA_{\mathrm{NIR}} + TOA_{\mathrm{RED}}} \tag{9}$$

$$\mathrm{NDVI}_{\rho} = \frac{\rho_{\mathrm{NIR}} - \rho_{\mathrm{RED}}}{\rho_{\mathrm{NIR}} + \rho_{\mathrm{RED}}} \tag{10}$$

$$r = \mathrm{NDVI}_{\mathrm{vege}} - \mathrm{NDVI}_{\mathrm{other}} \tag{11}$$

In the above formula, TOA_{NIR} and TOA_{RED}, respectively, denote apparent reflectance of near infrared and red bands from CCD data before atmospheric correction; ρ_{NIR} and ρ_{RED} refer to surface reflectance of near infrared and red bands from CCD after atmospheric correction, respectively; $\mathrm{NDVI}_{\mathrm{TOA}}$ and NDVI_{ρ} denote NDVI of CCD data of HJ-1 satellite before and after atmospheric correction; $\mathrm{NDVI}_{\mathrm{vege}}$ denotes NDVI of vegetation; $\mathrm{NDVI}_{\mathrm{other}}$ denotes NDVI of water or settlement place.

We randomly select one pixel from vegetation, water, and settlement place in the image, respectively. From Fig.6, we find that NDVI of the three pixels after atmospheric correction are larger than that before atmospheric correction. NDVI of vegetation and settlement place show increase while no evident difference is observed for the water. According to the three selected pixels, we calculate the mutual differences of NDVI for vegetation water, and settlement place that are 0.81 and 0.47, respectively, before atmospheric correction while the values change to 0.95 and 0.54 after atmospheric correction. Therefore, the difference of NDVI

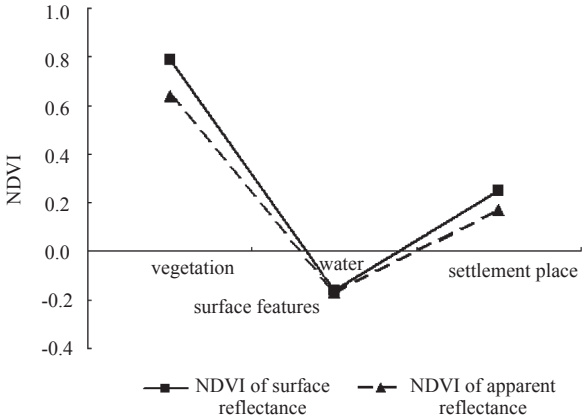

Fig. 6 The NDVI from the surface reflectance and the apparent reflectance

between vegetation and other objects after atmospheric correction is enhanced, indicating the atmospheric correction can highlight the vegetation information.

4 CONCLUSIONS

Timely monitoring environment and disaster in large-scale dynamics from HJ-1 satellite are inseparable from the quantitative analysis of remote sensing. Atmospheric correction is the basis for quantitative analysis and information extracted from satellite observations. The quality of surface reflectance data determines the accuracy, quality and availability of its derivative information. On the assumption that underlying surface is homogeneous Lambert, we perform atmospheric correction on CCD data of HJ-1 satellite through radioactive transfer model MODTRAN 4. Then, the effect of atmospheric correction on CCD data of HJ-1 satellite is analyzed in terms of the spectral curves, comparison with MODIS surface reflectance products, and the changes in normalized difference vegetation index (NDVI). The main procedures and conclusions are

1) The radioactive transfer process in the surface-atmosphere-remote sensor can be simulated by MODTRAN 4, thus we generate the look-up table of atmospheric correction on CCD data of HJ-1 satellite with different atmospheric parameters.

2) According to the look-up table, the atmospheric correction on CCD data is achieved pixel by pixel through VC^{++} programming. Analyzing from the spectral curves, we find atmospheric correction can largely eliminate the "increase" effect of atmospheric scattering in the visible bands.

3) Comparing atmospheric corrected CCD data of HJ-1 satellite with MODIS surface reflectance products, the result shows the surface reflectance of vegetation and settlement place from the two kinds of data is well consistent, and errors from the four bands of CCD data of HJ-1 satellite are within 20%.

4) NDVI of vegetation, water, and settlement place are larger after atmospheric correction, and the difference of NDVI between vegetation and other objects after atmospheric correction is enhanced.

REFERENCES

Berk A, Anderson G P, Acharya P K, Hoke M L, Chetwynd J H, Bernstein L S, Shettle E P, Matthew M W and Adler-Golden S M. 1999. MODTRAN4 User's Manual. Air Force Research Laboratory Space Vehicles Directorate Air Force Materiel Command Hanscom AFB, MA 01731–3010

Chi H K, Zhou G S, Xu Z Z, Xiao C W and Yuan W P. 2005. Apparent reflectance and its application in vegetation remote sensing. *Acta Phytoecologica Sinica*, **29**(1): 74–80

Ghulam A, Qin Q M and Zhu L J. 2004. 6S model based atmospheric correction of visible and near-infrared data and sensitivity analysis. *Acta Scientiarum Naturalium Universitatis Pekinensis*, **40**(4): 611–618

He L M, Wang H, Yan G J, Li X W, Zhu W J and Wang J D. 2003. Analysis and application for the empirical relative between aerosol optical depth and horizontal meteorological range. *Journal of Remote Sensing*, **7**(5): 372–378

Kaufman Y J, Tanré D, Remer L A, Vermote E F, Chu A and Holben B N. 1997. Operational remote sensing of tropospheric aerosol over land from EOS moderate resolution imaging spectroradiometer. *Journal of Geophysical Research*, **102**(D14): 17051–17067

King M D, Kaufman Y J, Menzel W P and Tanre D. 1992. Remote sensing of cloud, aerosol, and water vapor properties from the moderate resolution imaging spectrometer (MODIS). *IEEE Trans. on Geo. and Remote Sensing*, **30**(1): 2–27

Landsat Project Science Office. 2009. Landsat 7 Science Data User's Handbook. [2010–04–11] http://landsathandbook.gsfc.nasa.gov/handbook/handbook_htmls/chapter11/chapter11.html

Li G Y, Zhang Z Y, Zheng Y F and Liu X M. 2008. Atmospheric correction of MODIS and its application in cyanobacteria bloom monitoring in Lake Taihu. *Journal of Lake Sciences*, **20**(2): 160–166

Liang S L, Fallah-Adl H, Kalluri S, JáJá J, Kaufman Y J and Townshend J R G. 1997. An operational atmospheric correction algorithm for Landsat Thematic Mapper imagery over the land. *J Geophys Res*, **102**(D14): 17173–17186

Liang S L, Fang H L and Chen M Z. 2001. Atmospheric correction of Landsat ETM+ land surface imagery—Part I: methods. *IEEE Transactions on Geoscience and Remote Sensing*, **39**(11): 2490–2498

Matthew M W, Adler–Golden S M, Berk A, Felde G, Anderson G P, Gorodetsky D, Paswaters S and Shippert M. 2002. Atmospheric correction of spectral imagery: evaluation of the FLAASH algorithm with AVIRIS data. SPIE Proceeding of Algorithms and Technologies for Multispectral, Hyperspectral, and Ultraspectral Imagery IX [C]. Washington, DC, USA: IEEE Computer Society

Mi H and Zhang W Z. 2000. Practical Modern Statistical Analysis Method and SPSS Application. Beijing: Contemporary China Press

Peng G X, He Y H, Li J, Chen Y H and Lin W J. 2007. Study on CBERS-2's CCD image cross calibration and atmospheric correction. *Journal of Infrared and Millimeter Waves*, **26**(1): 22–25

Remerl L A, Tanré D and Kaufman Y J. MODIS ATBD: algorithm for remote sensing of tropospheric aerosol from MODIS: collection 5. Product ID: MOD04/MYD04–C005, 2006. 3–20

Vermote E F, Kotchenova S Y and Ray J P. 2008. MOD09 (Surface Reflectance) User's Guide. [2010–04–11]. http://modis–sr.ltdri.org

Wang Q and Wang W J. 2006. Macro Ecological Monitor Technology Research Based on Remote Sensing. Beijing: Chinese Environment Science Press

Wang Q, Zhang B, Wei Y C and Li X W. 2008. Water Environment Remote Sensing Monitor Test and Software Realization in Taihu Lake. Beijing: Science Press

Wu B Y, Li W, Chen H B, Li F, Zhang W X and Lu D R. 1998. Practical Algorithm for Atmospheric Radiative Transfer. Beijing: Meteorological Press

Xu C Y and Feng X Z. 2007. Atmospheric correction on TM image and its influence analysis on spectral response characteristic. *Journal of Nanjing University* (*Natural Sciences*), **43**(3): 309–317

Zhao C J, Song X Y, Wang J H, Liu L Y and Li C J. 2007. An algorithm based on 6S model for removing atmospheric effects form satellite imagery pixel by pixel. *Optical Technique*, **33**(1): 11–15

Zhao X, Liang S L, Liu S H, Wang J D, Qin J, Li Q and Li X W. 2007. Improvement of dark object method in atmospheric correction of hyperspectral remotely sensed data. *Science in China* (*Series D*), **37**(12): 1653–1659

Zhao Y S. 2003. Remote Sensing Application Analysis Theory and Method. Beijing: Science Press

HJ-1卫星CCD数据的大气校正及其效果分析

郑盛[1,2]，赵祥[3]，张颢[1]，何祺胜[1,2]，曹春香[1]，陈良富[1]

1. 遥感科学国家重点实验室 中国科学院遥感应用研究所，北京 100101；
2. 中国科学院 研究生院，北京 100049；
3. 北京师范大学 资源学院，北京 100875

摘 要：利用MODTRAN 4模型对地表-大气-遥感器之间的辐射传输过程进行模拟，模拟出对应大气参数下的表观辐亮度；利用模拟生成的大气校正查找表，逐像元对HJ-1卫星CCD数据进行大气校正；并从光谱曲线、与MODIS地表反射率产品比较、归一化植被指数(NDVI)三个方面，探讨了HJ-1卫星CCD数据大气校正效果。结果表明：(1) HJ-1卫星CCD数据的大气校正明显消除了大气在可见光波段的“增加”效应；(2) 大气校正后的HJ-1卫星CCD地表反射率数据与MODIS地表反射率产品在植被和居民地的地表反射率上具有很好的一致性，而且大气校正后的HJ-1卫星CCD数据4个波段在这两种地物上的误差大部分不超过20%；(3) 大气校正增大了植被NDVI和其他地物NDVI的差值，突出了植被信息。

关键词：HJ-1卫星，大气校正，MODTRAN 4，MODIS

中图分类号：P407.4/TP751.1 **文献标志码**：A

引用格式：郑盛，赵祥，张颢，何祺胜，曹春香，陈良富．2011．HJ-1卫星CCD数据的大气校正及其效果分析．遥感学报，**15**(4): 709–721

Zheng S, Zhao X, Zhang H, He Q S, Cao C X and Chen L F. 2011. Atmospheric correction on CCD data of HJ-1 satellite and analysis of its effect. *Journal of Remote Sensing*, **15**(4): 709–721

1 引 言

中国是自然灾害最为严重的国家之一，需要卫星遥感灾害监测系统加强对自然灾害监测预警预报能力。HJ-1卫星在这方面的作用尤为突出，它的主要任务是对环境污染、生态破坏和自然灾害进行大范围、全天候、全天时动态监测，同时对生态环境和自然灾害的发展变化趋势进行预测，对环境质量和灾害情况进行快速和科学的评估(王桥和王文杰，2006；王桥 等，2008)。HJ-1卫星的这些任务都离不开遥感的定量分析；比如在生态环境方面、监测植被指数、叶面积指数、土壤含水量等指标需要我们通过定量遥感的方法获取。在定量遥感中，遥感数据的大气校正是基本处理之一。由于大气分子、气溶胶的散射以及臭氧、水汽等气体的吸收，均会影响传感器接收到的信号，导致航空、航天遥感平台上的传感器接收到的地物信息不能真实地反映地表，而大量的反演算法建立在大气校正的地表反射率之上。因此大气校正是HJ-1卫星CCD数据地表参数定量反演的一个必备环节。

目前的大气校正模型大致可以归纳为：基于图像特征模型、地面线性回归经验模型、大气辐射传输理论模型3种(赵英时，2004)。基于图像特征模型仅利用遥感图像自身的信息，用该方法校正后的图像存在不同程度的噪声；地面线性回归经验模型需进行地面同步定标点的光谱测量，且要求地面定标点区域不宜过大，表面均匀；利用辐射传输模型反演地物反射率能较合理地描述大气散射、吸收等过程，它是基于准确的辐射传输模型和良好的大气参数获取方法；目前的辐射传输模型有MODTRAN、ACORN、HATCH等(Matthew 等，2002)。

收稿日期：2010-04-29；**修订日期**：2010-08-02

基金项目：国家重点基础研究发展计划(973计划)(编号：2007CB714402)；国家高科技研究发展计划(863计划)(编号：2008AA12Z107)；国家科技重大专项课题(编号：2008ZX10004-012)

第一作者简介：郑盛(1988—)，男，中国科学院遥感应用研究所硕士研究生，2009年毕业于中国地质大学(武汉)地理信息系统专业，现从事公共卫生领域空间信息技术应用和森林参数遥感反演方面的研究工作。E-mail: zhengsheng1213@163.com。

通信作者：张颢，E-mail: zhangh@irsa.ac.cn；曹春香，E-mail: cao413@irsa.ac.cn。

MODTRAN模型主要是对LOWTRAN模型的光谱分辨率进行了改进，它把光谱分辨率从20 cm^{-1}减少到2 cm^{-1}，发展了一种2 cm^{-1}光谱分辨率的分子吸收的算法和更新了对分子吸收的气压温度关系的处理，同时维持LOWTRAN 7的基本程序和使用结构。在程序处理上，MODTRAN基本保持了LOWTRAN结构，可作为中分辨率光谱计算能力的选择项而不干扰原来的执行。MODTRAN 比LOWTRAN 能更好地适用于高度高于30 km以上的路径。MODTRAN的输入参数从类型上讲，共分5类：运行参数、传感器的参数、大气参数、观测几何条件和地表参量(Berk 等，1999；吴北婴 等，1998)。

本文使用大气辐射传输模型MODTRAN 4实现了HJ-1卫星CCD数据的大气校正。利用MODTRAN 4模拟出对应大气参数下的表观辐亮度，并且建立大气校正查找表，然后逐像元校正HJ-1卫星CCD数据。在对一景HJ-1A CCD1的区域数据进行大气校正后，从典型地物光谱曲线、与MODIS地表反射率产品比较、NDVI3个方面，探讨了HJ-1卫星CCD数据大气校正的效果。

2 大气校正原理

遥感图像的成像过程包括了从地表到大气再到传感器的复杂传输过程。应用辐射传输模型MODTRAN 4对这传输过程进行模拟，可以反演HJ-1卫星CCD数据的地表反射率；其中主要涉及3个量，分别是表观辐亮度、表观反射率、地表反射率。

2.1 表观辐亮度计算

计算表观辐亮度就是用定标系数将图像上原始DN值转换为大气层外反射的表观辐亮度L；这是定量化的基础，遥感数据的应用很大程度上取决于定标系数的精度。其关系如式(1)所示：

$$L_\lambda = (DN / gain) + bias \tag{1}$$

式中，L_λ为测量的表观辐亮度；DN为原始影像象元灰度值；$gain$和$bias$为传感器对应的增益和偏差值。对于HJ-1卫星CCD数据，定标系数可以从下载数据的原数据文件中得到。大气校正效果分析中用到的数据是HJ-1A CCD1数据，其定标系数如表1。

表1 HJ-1A CCD1的定标系数

	Band1 (0.41—0.52 μm)	Band2 (0.52—0.60 μm)	Band3 (0.63—0.69 μm)	Band4 (0.76—0.90 μm)
Gain(DN/W·m^{-2}·sr^{-1}·μm^{-1})	0.5763	0.5410	0.6824	0.7209
Bias(W·m^{-2}·sr^{-1}·μm^{-1})	9.3183	9.1758	7.5072	4.1484

2.2 表观反射率算法

实现辐射定标后，采用式(2)将影像的表观辐亮度转换为表观反射率。式(2)中的表观辐亮度L_λ是大气层顶进入卫星传感器的光谱辐射亮度，它是来自地表和大气辐射亮度的总和；所以大气层顶的表观反射率也是地表反射率和大气反射率的总和(池宏康等，2005)。因此，通过对表观反射率和地表反射率的比较可以分析大气校正的效果。

$$\rho_\lambda = \frac{\pi L_\lambda d^2}{ESUN_\lambda \cos\theta_s} \tag{2}$$

式中，ρ_λ为波段λ的表观反射率；L_λ为波段λ的表观辐亮度；d为天文单位的日地距离，可对表2中的值进行插值获得(Landsat Project Science Office，2009)；$ESUN_\lambda$是波段λ处大气上界太阳光谱辐照度，其值可根据HJ-1卫星CCD数据的光谱响应函数与太阳照度数据获得，本文用到的$ESUN_\lambda$值如表3；θ_s是太阳天顶角(赵春江 等，2007)。

表2 天文单位的日地距离

天数	日地距离	天数	日地距离	天数	日地距离	天数	日地距离	天数	日地距离
1	0.98331	74	0.99446	152	1.01403	227	1.01281	305	0.99253
15	0.98365	91	0.99926	166	1.01577	242	1.00969	319	0.98916
32	0.98536	106	1.00353	182	1.01667	258	1.00566	335	0.98608
46	0.98774	121	1.00756	196	1.01646	274	1.00119	349	0.98426
60	0.99084	135	1.01087	213	1.01497	288	0.99718	365	0.98333

表3 HJ-1卫星CCD数据的大气上界太阳光谱辐照度(w/(m²·μm))

	Band1 (0.41—0.52 μm)	Band2 (0.52—0.60 μm)	Band3 (0.63—0.69 μm)	Band4 (0.76—0.90 μm)
HJ-1A CCD1	1914.324	1825.419	1542.664	1073.826
HJ-1A CCD2	1929.810	1831.144	1549.824	1078.317
HJ-1B CCD1	1902.188	1833.626	1566.714	1077.085
HJ-1B CCD2	1922.897	1823.985	1553.201	1074.544

2.3 地表反射率算法

基于辐射传输理论，假设地面像元为均一、朗伯地表时，则在大气上界传感器接收到的光谱辐亮度可以表示为(Liang 等，1997)：

$$L_m = L_0 + \frac{\rho}{1-s\cdot\rho}\cdot\frac{TF_d}{\pi} \quad (3)$$

式中，L_0表示零地表反射时大气引起的程辐射，T表示地表到传感器的透过率，s为大气底层球面反照率，ρ为像元反射率，F_d为到达地表的下行辐射通量密度(赵祥 等，2007)。

对HJ-1卫星CCD数据进行大气校正，利用式3由表观辐亮度L_m反推出地表反射率ρ一般分两步：第一步是获取相应的大气参数。太阳天顶角可从头文件中间接获得；卫星天顶角可从下载的卫星天顶角文件中获得；水平气象视距可从气溶胶光学厚度转化而来(何立明 等，2003)，气溶胶光学厚度的获得方法较多，可以参考Kaufman等人(1997)建立的暗像元算法来反演气溶胶或则直接下载MODIS的日气溶胶产品来大致估计研究区域的气溶胶光学厚度。第二步是根据式(3)，反推出地表反射率。首先在一定的大气参数条件下，MODTRAN 4运行3次，这3次运行分别假设3个地表反射率(ρ=0，0.5，0.8)，从运行结果中可以得到3个模拟的表观辐亮度L_m。将3组对应的地表反射率ρ和表观辐亮度L_m代入式(3)中，可以建立一个关于变量L_0，s及TF_d/π的三元一次方程组，解方程组，求出一组与该大气参数对应的L_0，s及TF_d/π值。这样,对于大气参数、地表反射率ρ和表观辐亮度L_m这3个量，只要知道其中两个，就可推出第3个量(Liang 等，2001)。

本研究设定下垫面为均一、朗伯地表,利用MODTRAN 4建立大气校正查找表。由于HJ-1卫星CCD数据4个波段的光谱响应函数不同，所以针对每个波段建立大气校正查找表。大气校正通常需要考虑到水平气象视距、水汽含量、太阳天顶角、卫星天顶角等参数的变化。对于HJ-1卫星CCD数据，它所处波段几乎不涉及水汽吸收带，而且受水汽的影响很小，因此没有考虑水汽影响。在求地表反射率的查找表中，在参照Remer1(2006)建立的MODIS气溶胶反演的查找表基础上，为了提高大气校正的精度，又内插了些数值。本文中用到的4个查找表，其自变量都是大气模式、卫星天顶角、太阳天顶角和水平气象视距；因变量都是式(3)中的L_0，s及TF_d/π。大气模式为2和3，分别代表中纬度夏季大气和中纬度冬季大气；卫星天顶角是0°，8°，16°，24°，32°；太阳天顶角是0.0°，6.0°，12.0°，24.0°，35.2°，48.0°，54.0°，60.0°，66.0°；水平气象视距为0.4 km，0.7 km，0.9 km，1.2 km，1.4 km，1.7 km，2 km，2.3 km，2.6 km，3.1 km，3.5 km，4.0 km，4.4 km，5.2 km，6.1 km，7.0 km，7.9 km，9.6 km，11.4 km，13.1 km，16.6 km，20.2 km，23.7 km，27.2 km，33.8 km，40.4 km，53.6 km，66.8 km，80.0 km。

2.4 气溶胶光学厚度与水平气象视距转换

气溶胶光学厚度在大气校正中被广泛使用，比如，MODIS气溶胶光学厚度产品作为MODIS数据大气订正的输入参数之一(King 等，1992)。而在MODTRAN 4中，输入参数是水平气象视距；而且本文的大气校正查找表是以水平气象视距作为自变量之一的。因此在做HJ-1卫星CCD数据大气校正的时候，需要将气溶胶光学厚度转化为水平气象视距。根据Lambert—Beer定律，可以得到(何立明 等，2003)

$$\tau_a = \int_{z_1}^{z_2} N(z,VIS)\cdot EXT(\lambda)m_a(z)\mathrm{d}z = -\ln T_a \quad (4)$$

式中τ_a为气溶胶光学厚度，$N(z, VIS)$为与高度(z)和水平气象视距有关的气溶胶粒子密度系数，$EXT(\lambda)$为消光系数，λ为波长，$m_a(z)$为大气质量，T_a为气溶胶引起的透过率(赵祥 等，2007)。利用MODTRAN 4可以计算出不同水平气象视距、季节、水汽量和气溶胶模式下气溶胶的透过率，进而得到气溶胶光学厚度，这样就建立了水平气象视距和气溶胶光学厚度的关系。由于水汽对两者关系的影响非常小(何立明 等，2003)，所以就没考虑水汽的变化，气溶胶模式选择

乡村气溶胶，季节分为春夏和秋冬，这样就可以得到在乡村气溶胶下，两个不同季节中水平气象视距下和气溶胶光学厚度的关系。图1给出了乡村气溶胶模式下，夏季水平气象视距与气溶胶光学厚度之间拟合的关系曲线；图2给出了乡村气溶胶模式下，夏季水平气象视距和气溶胶光学厚度倒数之间拟合的关系曲线。利用SPSS软件中的线性回归分析(米红和张文璋，2000)即可获得气溶胶光学厚度的倒数和水平气象视距线性之间拟合关系曲线的系数。

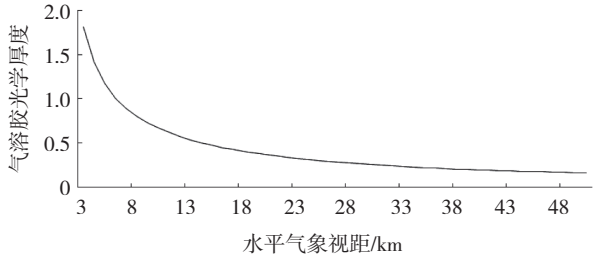

图1 乡村气溶胶、夏季水平气象视距与气溶胶光学厚度之间拟合的关系曲线

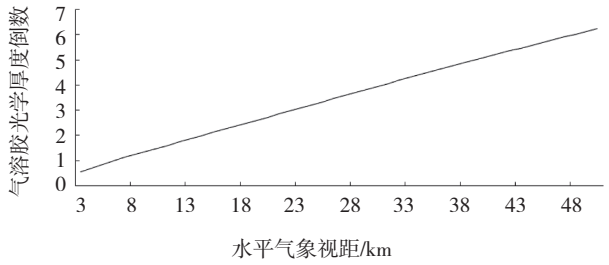

图2 乡村气溶胶、夏季水平气象视距与气溶胶光学厚度倒数之间拟合的关系曲线

最终的拟合结果如下：

$$\text{春夏：}\frac{1}{t(550)}=0.1202V+0.29735 \tag{5}$$

$$\text{秋冬：}\frac{1}{t(550)}=0.1419V+0.1377 \tag{6}$$

式中，$t(550)$表示550 nm处的气溶胶光学厚度，V代表水平气象视距(km)。

3 效果分析

本文选取2009年5月9日HJ-1A CCD1相机在浙江湖州成像的图像进行地表反射率反演。图像中的研究区域在北纬30° 48′，东经120° 6′附近，大气模式是中纬度夏季大气，气溶胶模式为乡村气溶胶模式，过顶时太阳天顶角为18° 36′。根据研究区域在HJ-1卫星CCD数据中的行列数，从下载的卫星天顶角文件中查找得到此处卫星天顶角为9° 。根据MODIS的气溶胶光学厚度产品得到在此经纬度上的气溶胶厚度值，其值为0.325，转换成水平气象视距是23.12 km。根据这些大气参数和利用MODTRAN 4建立的大气校正查找表，利用VC^{++}编程实现HJ-1卫星CCD数据的大气校正。

3.1 大气校正对地物光谱特征的影响

大气以两种方式影响着遥感器所记录的地面目标的“亮度”或“辐射亮度”。一是大气的吸收、散射作用使到达地面目标的太阳辐射能量和从目标反射的能量均衰减；二是大气本身作为一个反射体(散射体)的程辐射使能量增加，但是它与所探测的地面信息无关(赵英时，2004)。对可见光波段而言，主要受到第二种方式的影响。本文分别选取水体、植被和居民地这3种典型地物对表观反射率图像和地表反射率图像的光谱曲线进行分析。

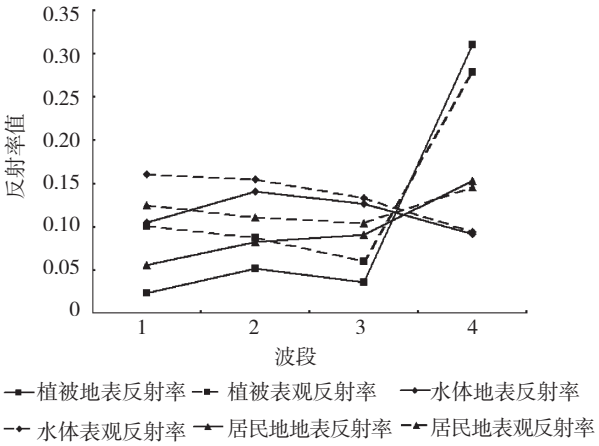

图3 地表反射率和表观反射率图像的地物光谱曲线

由图3可以看出，3种地物的表观反射率在蓝波段(第1波段)，绿波段(第2波段)，红波段(第3波段)的光谱响应值都比地表反射率大。以植被的反射率为例，利用式(7)计算出大气校正前后变化率最大的为蓝波段的76.6%，次之为绿波段的41.1%，然后是红波段的40.0%。这是因为大气散射的选择性，它对短波影响大，对长波影响小；大气校正消除了大气散射在可见光波段的“增加”效应。

$$k=\frac{|\rho_s-\rho_{toa}|}{\rho_{toa}}\times 100\% \tag{7}$$

式中，k表示变化率，ρ_s表示大气校正后的地表反射率，ρ_{toa}表示大气校正前的表观反射率，符号“||”表

示取绝对值。

3.2 与MODIS地表反射率产品比较

为了进一步验证大气校正效果，将大气校正后的HJ-1卫星CCD数据与MODIS的地表反射率产品进行比较。虽然MODIS地表反射率产品的空间分辨率比HJ-1卫星CCD数据的大，但研究区域有大范围的植被和居民地，在两种数据中均可找到由其中一种地物构成的像元；所以比较两种数据在研究区域的地表反射率时很少受空间分辨率差异的影响。MODIS地表反射率产品一共有5种，本文用到MOD09GA产品和MOD09GQ产品(Vermote 等，2008)。MOD09GA产品的空间分辨率为500 m，含有7个波段；为提高验证精度，本文只用到蓝和绿两个波段，而红和近红外两个波段由空间分辨率为250 m，MOD09GQ产品来替代；MOD09GA产品和MOD09GQ产品的获取时间均是2009年5月9日，和HJ-1A CCD1数据获取时间是一样的。

在将大气校正后HJ-1卫星CCD数据和MODIS的地表反射率产品比较前，要对MODIS地表反射率产品进行预处理。首先将MODIS地表反射率产品转化为WGS84椭球下的UTM投影，然后裁剪出研究区域；再对空间分辨率为500 m的蓝、绿波段进行空间重采样，使其与MOD09GQ产品的空间分辨率一致，最后合并4个波段形成一个影像文件，处理的流程如图4。

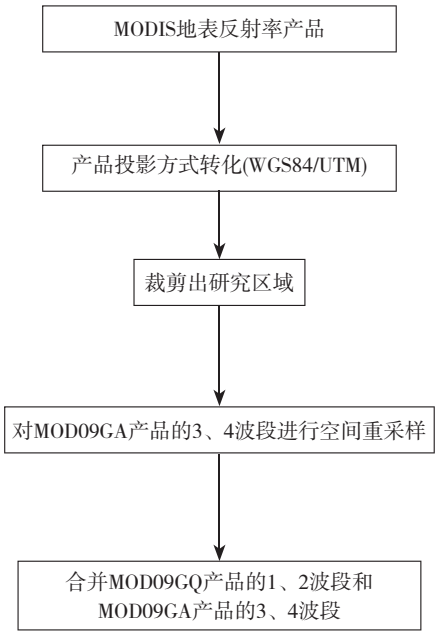

图4 MODIS地表反射率产品预处理流程图

将大气校正后HJ-1卫星CCD数据的空间分辨率重采样MOD09GQ产品的分辨率，然后进行重采样后HJ-1卫星CCD数据与处理好的MODIS数据的比较。在研究区域的植被、居民地两种地物中分别随机选取一个像元；获得两种数据分别在这两个像元上的反射率值，两种数据的地表反射率如图5。从图中可以看出两种数据在两种地物的地表反射率上都具有很好的一致性。根据式(8)，计算出的误差如表4；从表中可以看出，植被和居民地在4个波段上的误差大部分在20%以内。

$$e=\frac{|\rho_{\mathrm{HJCCD}}-\rho_{\mathrm{MODIS}}|}{\rho_{\mathrm{MODIS}}}\times 100\% \tag{8}$$

式中，e表示误差，ρ_{HJCCD}表示HJ-1卫星CCD数据的地表反射率，ρ_{MODIS}表示MODIS的地表反射率，符号“||”表示取绝对值。

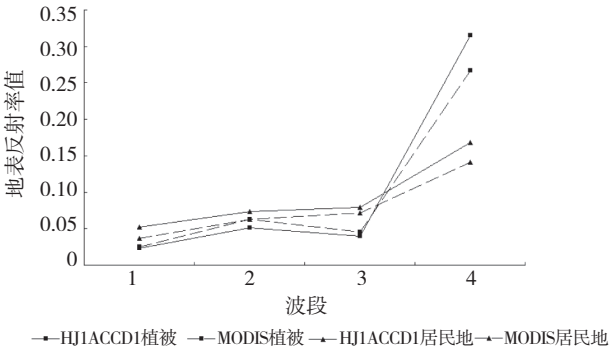

图5 HJ-1A CCD1与MODIS的植被地表反射率2009–05–09

表4 HJ-1A CCD1与MODIS的地表反射率之间的误差

/%

	波段1	波段2	波段3	波段4
植被	7.4	18.6	12.1	18.0
居民地	42.1	17.4	11.4	18.8

3.3 大气校正对NDVI的影响

为了验证HJ-1卫星CCD数据大气校正的效果，对校正前后的归一化植被指数NDVI的变化进行了比较，因为植被指数是定量遥感中常用的变量，许多遥感模型和以遥感信息为驱动变量的生态学模型都需要植被指数的参与(彭光雄 等，2007)。已有的一些研究(阿布都瓦斯提 等，2004；徐春燕和冯学智，2007；李国砚 等，2008)表明利用NDVI能检测大气校正的效果。大气校正前后NDVI的计算公式如下：

$$\mathrm{NDVI}_{\mathrm{TOA}}=\frac{TOA_{\mathrm{NIR}}-TOA_{\mathrm{RED}}}{TOA_{\mathrm{NIR}}+TOA_{\mathrm{RED}}} \tag{9}$$

$$\mathrm{NDVI}_{\rho}=\frac{\rho_{\mathrm{NIR}}-\rho_{\mathrm{RED}}}{\rho_{\mathrm{NIR}}+\rho_{\mathrm{RED}}} \tag{10}$$

$$r=\mathrm{NDVI}_{\mathrm{vege}}-\mathrm{NDVI}_{\mathrm{other}} \tag{11}$$

式中，TOA_{NIR}和TOA_{RED}分别表示大气校正前HJ-1卫星CCD数据近红外波段和红波段的表观反射率，ρ_{NIR}和ρ_{RED}分别表示大气校正后HJ-1卫星CCD数据近红外波段和红波段的地表反射率，$\mathrm{NDVI}_{\mathrm{TOA}}$和$\mathrm{NDVI}_{\rho}$分别表示大气校正前后HJ-1卫星CCD数据的NDVI，$\mathrm{NDVI}_{\mathrm{vege}}$表示植被的NDVI，$\mathrm{NDVI}_{\mathrm{other}}$表示水体或则居民地的NDVI。

分别在图像的植被、水体、居民地3种地物中随机选取1个像元；从图6可以看出，3个像元的NDVI在大气校正后的值均比在大气校正前的大，除了水体的增幅不怎么明显外，植被和居民地的增幅都是很明显的。根据选取的3个像元，利用式(11)计算出大气校正前$\mathrm{NDVI}_{\mathrm{vege}}$与$\mathrm{NDVI}_{\mathrm{other}}$差值分别为0.81，0.47；大气校正后$\mathrm{NDVI}_{\mathrm{vege}}$与$\mathrm{NDVI}_{\mathrm{other}}$差值分别为0.95，0.54；因此大气校正增大了$\mathrm{NDVI}_{\mathrm{vege}}$和其他地物NDVI的差值，有利于区分植被信息和其他地物信息。

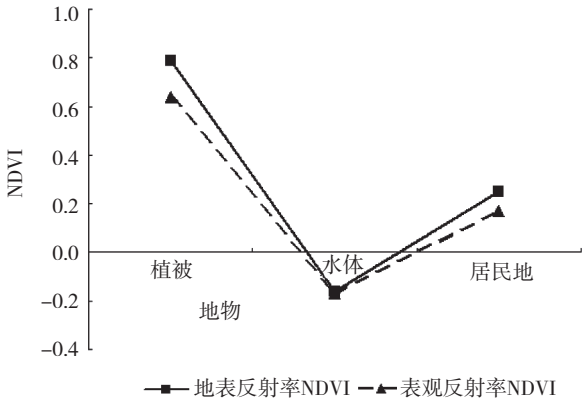

图6 地表反射率和表观反射率的NDVI

4 结 论

HJ-1卫星实现的大范围、及时、动态的环境和灾害监测都离不开遥感的定量分析。大气校正是HJ-1卫星CCD数据进行定量分析和信息提取的基础，而且地表反射率数据质量决定了其衍生信息的精度、质量与可用性。本文假设地面像元为均一、朗伯地表，使用辐射传输模型MODTRAN 4实现了HJ-1卫星CCD数据的大气校正；然后从光谱曲线、与MODIS地表反射率产品比较、NDVI 3个方面探讨了HJ-1卫星CCD数据大气校正的效果。主要的工作和结论是：

(1)利用MODTRAN 4对大气-地表-遥感器之间的辐射传输过程进行模拟，生成在不同大气参数下，适用于HJ-1卫星CCD数据大气校正的查找表(LUT)。

(2)根据查找表，利用VC^{++}编程实现逐像元大气校正。从光谱曲线上分析，HJ-1卫星CCD数据的大气校正明显消除了大气在可见光波段的“增加”效应。

(3)将大气校正后的HJ-1卫星CCD数据与MODIS的地表反射率产品进行比较，结果表明两种数据在植被和居民地的地表反射率上都具有很好的一致性，而且4个波段在这两种地物上的误差大部分不超过20%。

(4)大气校正后植被，水体，居民地的NDVI均有所增加；大气校正增大了植被NDVI和其他地物NDVI的差值，突出了植被信息。

REFERENCES

Berk A, Anderson G P, Acharya P K, Hoke M L, Chetwynd J H, Bernstein L S, Shettle E P, Matthew M W and Adler-Golden S M. 1999. MODTRAN4 User’s Manual. Air Force Research Laboratory Space Vehicles Directorate Air Force Materiel Command Hanscom AFB, MA 01731–3010

Chi H K, Zhou G S, Xu Z Z, Xiao C W and Yuan W P. 2005. Apparent reflectance and its application in vegetation remote sensing. *Acta Phytoecologica Sinica*, **29**(1): 74–80

Ghulam A, Qin Q M and Zhu L J. 2004. 6S model based atmospheric correction of visible and near-infrared data and sensitivity analysis. *Acta Scientiarum Naturalium Universitatis Pekinensis*, **40**(4): 611–618

He L M, Wang H, Yan G J, Li X W, Zhu W J and Wang J D. 2003. Analysis and application for the empirical relative between aerosol optical depth and horizontal meteorological range. *Journal of Remote Sensing*, **7**(5): 372–378

Kaufman Y J, Tanré D, Remer L A, Vermote E F, Chu A and Holben B N. 1997. Operational remote sensing of tropospheric aerosol over land from EOS moderate resolution imaging spectroradiometer. *Journal of Geophysical Research*, **102**(D14): 17051–17067

King M D, Kaufman Y J, Menzel W P and Tanre D. 1992. Remote sensing of cloud, aerosol, and water vapor properties from the moderate resolution imaging spectrometer (MODIS). *IEEE Trans. on Geo. and Remote Sensing*, **30**(1): 2–27

Li G Y, Zhang Z Y, Zheng Y F and Liu X M. 2008. Atmospheric correction of MODIS and its application in cyanobacteria bloom monitoring in Lake Taihu. *Journal of Lake Sciences*, **20**(2): 160–166

Landsat Project Science Office. 2009. Landsat 7 Science Data User’s Handbook. [2010–04–11] http://landsathandbook.gsfc.nasa.gov/handbook/handbook_htmls/chapter11/chapter11.html

Liang S L, Fallah–Adl H, Kalluri S, JáJá J, Kaufman Y J and Townshend J R G. 1997. An operational atmospheric correction algorithm for Landsat Thematic Mapper imagery over the land. *J Geophys Res*, **102**(D14): 17173–17186

Liang S L, Fang H L and Chen M Z. 2001. Atmospheric correction of Landsat ETM+ land surface imagery—Part I: methods. *IEEE Transactions on Geoscience and Remote Sensing*, **39**(11): 2490–2498

Matthew M W, Adler-Golden S M, Berk A, Felde G, Anderson G P, Gorodetsky D, Paswaters S and Shippert M. 2002. Atmospheric correction of spectral imagery: evaluation of the FLAASH algorithm with AVIRIS data. SPIE Proceeding of Algorithms and Technologies for Multispectral, Hyperspectral, and Ultraspectral Imagery IX [C]. Washington, DC, USA: IEEE Computer Society

Mi H and Zhang W Z. 2000. Practical Modern Statistical Analysis Method and SPSS Application. Beijing: Contemporary China Press

Peng G X, He Y H, Li J, Chen Y H and Lin W J. 2007. Study on CBERS-2's CCD image cross calibration and atmospheric correction. *Journal of Infrared and Millimeter Waves*, **26**(1): 22–25

Remerl L A, Tanré D and Kaufman Y J. MODIS ATBD: algorithm for remote sensing of tropospheric aerosol from MODIS: collection 5. Product ID: MOD04/MYD04–C005, 2006. 3–20

Vermote E F, Kotchenova S Y and Ray J P. 2008. MOD09 (Surface Reflectance) User's Guide. [2010–04–11]. http://modis–sr.ltdri.org

Wang Q and Wang W J. 2006. Macro Ecological Monitor Technology Research Based on Remote Sensing. Beijing: Chinese Environment Science Press

Wang Q, Zhang B, Wei Y C and Li X W. 2008. Water Environment Remote Sensing Monitor Test and Software Realization in Taihu Lake. Beijing: Science Press

Wu B Y, Li W, Chen H B, Li F, Zhang W X and Lu D R. 1998. Practical Algorithm for Atmospheric Radiative Transfer. Beijing: Meteorological Press

Xu C Y and Feng X Z. 2007. Atmospheric correction on TM image and its influence analysis on spectral response characteristic. *Journal of Nanjing University* (*Natural Sciences*), **43**(3): 309–317

Zhao C J, Song X Y, Wang J H, Liu L Y and Li C J. 2007. An algorithm based on 6S model for removing atmospheric effects form satellite imagery pixel by pixel. *Optical Technique*, **33**(1): 11–15

Zhao X, Liang S L, Liu S H, Wang J D, Qin J, Li Q and Li X W. 2007. Improvement of dark object method in atmospheric correction of hyperspectral remotely sensed data. *Science in China* (*Series D*), **37**(12): 1653–1659

Zhao Y S. 2003. Remote Sensing Application Analysis Theory and Method. Beijing: Science Press

附中文参考文献

阿布都瓦斯提·吾拉木，秦其明，朱犁江. 2004. 基于6S 模型的可见光、近红外遥感数据的大气校正. 北京大学学报(自然科学版)，**40**(4)：611–618

池宏康，周广胜，许振柱，肖春旺，袁文平. 2005. 表观反射率及其在植被遥感中的应用. 植物生态学报，**29**(1)：74–80

何立明，王华，阎广建，李小文，朱文娇，王锦地. 2003. 气溶胶光学厚度与水平气象视距相互转换的经验公式及其应用. 遥感学报，**7**(5)：372–378

李国砚，张仲元，郑艳芬，刘晓玫. 2008. MODIS 影像的大气校正及在太湖蓝藻监测中的应用. 湖泊科学，**20**(2)：160–166

米红，张文璋. 2000. 实用现代统计分析方法与SPSS应用. 北京：当代中国出版社

彭光雄，何宇华，李京，陈云浩，林文娟. 2007. 中巴地球资源02星CCD图像交叉定标与大气校正研究. 红外与毫米波学报，**26**(1)：22–25

王桥，王文杰. 2006. 基于遥感的宏观生态监控技术研究. 北京：中国环境科学出版社

王桥，张兵，韦玉春，李旭文. 2008. 太湖水体环境遥感监测试验及其软件实现. 北京：科学出版社

吴北婴，李卫，陈洪滨，李放，章文星，吕达仁. 1998. 大气辐射传输实用算法. 北京：气象出版社

徐春燕，冯学智. 2007. TM图像大气校正及其对地物光谱响应特征的影响分析. 南京大学学报(自然科学)，**43**(3)：309–317(请调整本条文献顺序)

赵春江，宋晓宇，王纪华，刘良云，李存军. 2007. 基于6S模型的遥感影像逐像元大气纠正算法. 光学技术，**33**(1)：11–15

赵祥，梁顺林，刘素红，王锦地，秦军，厉青，李小文. 2007. 高光谱遥感数据的改正暗目标大气校正方法研究. 中国科学D辑，**37**(12)：1653–1659

赵英时. 2003. 遥感应用分析原理与方法. 北京：科学出版社